

# Feedforward Inversion Control of DC/DC Dual-Bridge Series Resonant Converter in Buck and Boost Modes

Alex Borisevich, akpc806b@gmail.com,  
 Filipp Gleyzer, gleyzerf@smccd.edu,  
 Valeria Gavrilenko

June 7, 2022

## Abstract

In the paper, a nonlinear inversion technique for the steady-state model of the active dual-bridge series resonant converter is presented. The obtained control strategy allows cycle averaged output current regulation and performs waveform alignment for the controllable achievement of ZVS and synchronous rectification. The control is valid both for voltage buck and boost operating modes, as well as for low-power operation at a fixed frequency. Robustness of the control is studied by simulations with external linear control loops.

## 1 Introduction

The dual-bridge series resonant converter (DB SRC) [1], which shares some similarities with the standard full-bridge DC/DC series resonant converters (like LLC), still has some unique features due to the secondary-side bridge, such as the capability of bidirectional power flow and voltage boost operation. Such type of converter topology is particularly promising for electric vehicles chargers applications [1-3], including off-board charging stations and on-board charger modules with an ability for bidirectional vehicle-to-grid power flow. Additionally, many other power electronics applications like battery energy storage and DC line power transmission are target areas of DB SRC topology.

The modulation scheme for DB SRC usually enables pure ZVS on the primary side, and combined ZVS/ZCS on the secondary side, and allows for an efficient utilization of the primary side switches with wide changes in load or supply voltage, which is preferred in many applications [2]. The impedance of series resonant tank is determined by value of inductor and capacitor together with the switching frequency. Therefore, it can operate at higher frequency under high power level [3] than just dual active bridge topologies without resonant capacitor, which allows more compact magnetic designs.

All the switches in the two bridges work with 50

Comparing to LLC converter, the DB SRC converter requires more advanced control strategy since the DC gain of a LC series resonant converter is always less than unity with a passive (diode) rectifier. Also at light-load condition, the impedance of the load is very large compared to the impedance of the resonant network, so all the input voltage is imposed on the load [5]. Thus an actively controlled full bridge on the secondary side is essential in order to achieve voltage gain higher than one and regulate power delivered at light load.

The operating modes and controls principles of the converter have been extensively analyzed in [6, 7, 8]. The published modeling efforts can be classified into three categories:

1. Fundamental harmonics approximation (FHA) approach [6, 7, 8, 9, 10], consisting of replacement the rectangular voltage waveforms by sinusoidal approximations, calculated accordingly. The same result can be achieved if output and input voltages are represented by rotating vectors using phasor diagrams. If the analysis of a converter is performed not too far from its resonant frequency, then the resonant tank current consists primary a fundamental harmonic, and this method produces reasonable well approximations. Another advantage of FHA is that this method ends up with trigonometric functions over switching parameters, where analytical results can be relevantly easy to obtain.

2. State-plane trajectory analysis pioneered by R. Oruganti [12] and used by many followers [13, 14, 15, 16].. The key idea is to represent the converter dynamics in two-dimensional plane of resonant inductor current and resonant capacitor voltage. The analysis is greatly simplified by the fact that with a proper normalization the state plane trajectory of voltage step response of an undamped LC circuit is circular and is centered at the DC solution of the circuit. Thus, accurate and purely geometric analysis can be performed for arbitrary operating point and switching pattern. The downside of this method is that the closed form solutions are becoming very complicated with less trivial PWM patterns (like combined duty cycle and phase shift control), and also for multi-element resonant converters, more state variables need to be analyzed and more complicated calculation is required.

3. Piece-wise time-domain modeling. This technique is originally applied to the dual-bridge converters [17, 18, 19, 20] without a resonant tank, where transformer current is a straight line between switching events. Thus each time interval between switching of bridges can be analyzed separately, and then final waveform is obtained by gluing together transient responses for consequential time intervals. This technique can be directly obtained to series resonant converter operating very far from resonant frequency, where resonant tank current is piece-wise linear. Also it is not very hard to obtain a closed form solutions for different operating modes of series resonant converter [21].

Despite pretty diverse modeling and control techniques published, there are still some gaps, namely:

- there is no model and corresponding nonlinear control problem formulated addressing both produced output power and optimal regime of operation in terms of the waveform timings,
- all three modes of operation, namely variable frequency buck, variable frequency boost and fixed frequency low power operation are not being considered in a single model.

In this work we will derive nonlinear control affine model of the converter, which describes large signal operation over whole frequency range above resonance and in all possible operation modes as buck, boost and low power. This model also demonstrates interesting control properties of the converter like high nonlinearity respect to the switching parameters, singularity of output current surface between buck and boost modes, and also holonomic constraints for control variables. We believe that this model could be an another practical benchmark for many advanced nonlinear control techniques such as feedback linearization, differential flatness theory, optimal control, etc.

## 2 Background

This section is a recall of previously published results, and the model [22] in particularly.

### 2.1 The converter topology

The basic electrical circuit of the series LC resonant DC/DC converter is shown in Figure 1.

The circuit consists of two full (H) transistor bridges: input bridge with switches  $S_1$ – $S_4$  and output bridge with switches  $S_5$ – $S_8$ . The output bridge is directly connected to the secondary side of transformer TX. The input bridge is connected to the transformer TX through capacitor C. Simple representation of transformer is used with magnetizing inductance  $L_m$ , leakage inductance  $L$  and an ideal transformer with turns ratio  $n$ .

If the magnetizing inductance  $L_m$  is much larger than leakage inductance  $L$ :  $L_m \gg L$ , then there is almost no circulating magnetizing current in the circuit. This has an advantage because all the current from primary side is flowing to the secondary side which increases the efficiency. Also the current in secondary side of transformer is in phase with primary side, which allows easy synchronous rectification by measuring current only in primary side.

By eliminating  $L_m$  from the circuit, we can spot that the stray inductance  $L$  together with capacitor  $C$  forms LC resonant tank. Also ideal transformer can be embedded into secondary bridge for simplification of analysis. Thus we can obtain a black-box circuit presented in Figure ??.

### 2.2 The waveforms

Let's consider voltages  $v_{in}(t)$  and  $v_{out}(t)$  at output terminals of bridges. In the circuit 1 this corresponds to voltage measured between points A–B for input bridge and scaled  $n$  times voltages between points C–D

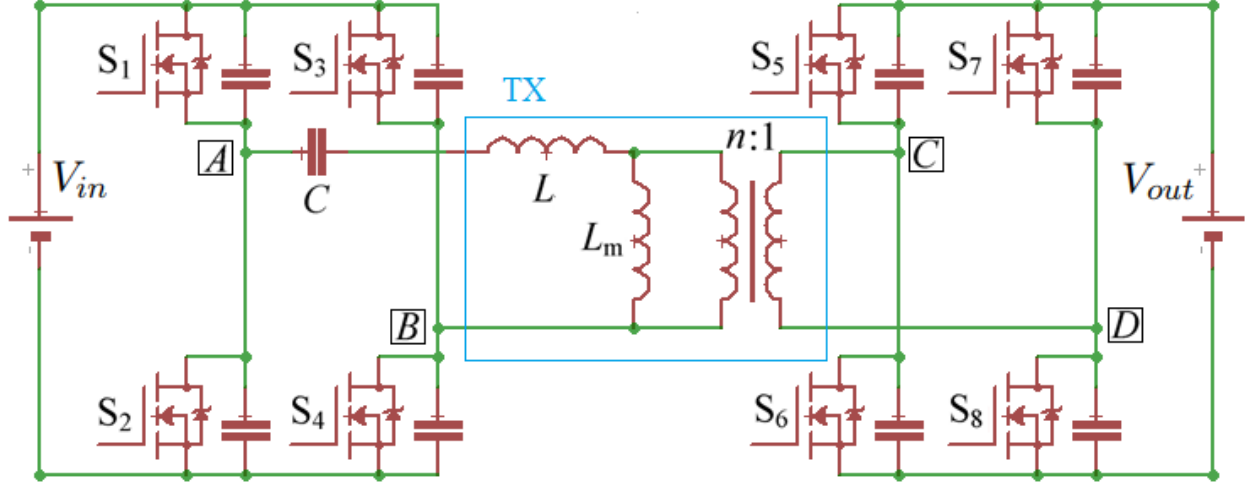


Figure 1: DC/DC circuit.

for output bridge. Effectively, these are the voltages applied to LC-circuit. Figure 2 shows the real (top) and rectangular approximated (bottom) voltages.

Lets consider rectangular approximated voltages  $u_{in}(t)$  and  $u_{out}(t)$  for easier explanation of controllable switching parameters:

- The input voltage source is producing rectangular pulses with controlled duty cycle and frequency. The amplitude of pulse is  $V_{in}$  and the on-time is  $d$  (in radians, i.e.  $d = \pi$  is full square wave). The angular frequency is  $\omega$ , which is equivalent to frequency  $F = 1/T$  in Hz.
- The output voltage source is producing rectangular pulses with amplitude  $nV_{out}$  with controlled duty cycle, frequency, and phase shift respect to input bridge. The reciprocal of duty cycle, the off-time or short time is  $s$  (defined in radians,  $s = \pi$  means that secondary side of transformer is fully shorted). The off-time is always located at the beginning of switching cycle. The phase shift between the output bridge switching cycle and input bridge switching cycle is  $\beta$ .

The output to input voltage ratio is defined as converter voltage gain:

$$G = \frac{nV_{out}}{V_{in}} \quad (1)$$

The real waveforms are looking differently than approximated ones because of dead times, which are smoothing rising and falling edges of the switching pulses. Since this DC/DC belongs to the class of resonant converters, energy is also transferring during the dead time, and the dead time is an essential phase of converter operation.

The duration of dead-time for input bridge is  $T_D^{in}$ , and the duration of dead-time for output bridge is  $T_D^{out}$ .

### 2.3 The model

The converter model obtained in [22] can be summarized as:

$$W = \frac{n}{2\pi^2} \frac{\sqrt{A(\beta, s, G)^2 + B(\beta, s, G)^2}}{Z(\omega)} (\cos(s + \delta) + \cos \delta) \quad (2)$$

$$\delta = \beta - \frac{\pi}{2} + \phi_0(\beta, s, G)$$

$$\sigma = \frac{\pi}{2} - \phi_0(\beta, s, G)$$

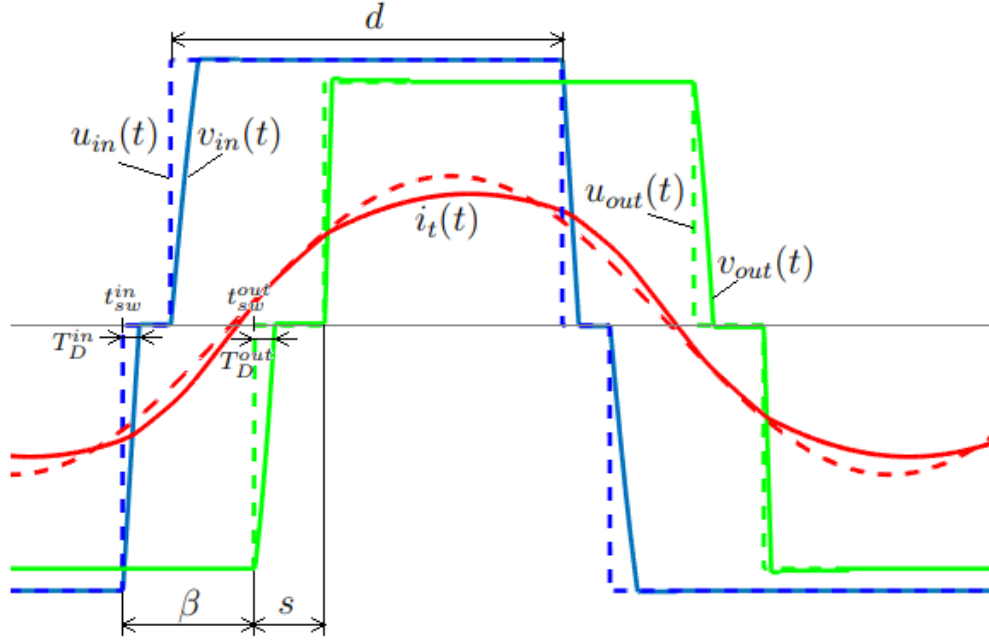


Figure 2: Real and approximated voltages applied to resonant LC circuit and commutation parameters.

where coefficients  $A(\beta, s, G)$  and  $B(\beta, s, G)$  along with  $\phi_0(\beta, s, G)$  are given as

$$\begin{aligned} A &= 4 \sin d + 4G \sin(\beta + s) + 4G \sin \beta \\ B &= 4 - 4G \cos(\beta + s) - 4G \cos \beta - 4 \cos d \\ \phi_0 &= \text{atan}(A, B) \end{aligned} \quad (3)$$

and  $Z(\omega)$  is resonant LC tank impedance:

$$Z(\omega) = X_L - X_C = \omega L - \frac{1}{\omega C} \quad (4)$$

and additionally

$$\sigma + \delta = \beta \quad (5)$$

$$W = \frac{I_{out}}{V_{in}} \quad (6)$$

## 2.4 The output control problem

The output control problem is formulated as achieving referenced transconductance  $W_{ref}$ , minimizing reactive power by optimal synchronous rectification and achieving ZVS for both bridges, in the input bridge particularly:

$$\begin{aligned} W &= W_{ref} \\ \delta &= 0 \\ \sigma &\geq \sigma_{min} > 0 \end{aligned} \quad (7)$$

where  $W_{ref}$  is desired (reference) output transconductance, i.e. output current normalized to input voltage.

An additional optimality condition for state  $s$  should be imposed:

$$s \rightarrow \min \quad (8)$$

which minimizes the tank current by minimal amount of secondary side shorting (boosting).

### 3 Synchronous rectification constraint $\delta = 0$

Let's consider second equation in (2). In order to satisfy the control goal  $\delta = 0$  for synchronous rectification, the following should be true:

$$\delta = \beta - \frac{\pi}{2} + \phi_0(\beta, s, G) = 0 \quad (9)$$

or

$$\beta = \frac{\pi}{2} - \phi_0(\beta, s, G) \quad (10)$$

which gives us

$$\beta = \sigma = \frac{\pi}{2} - \phi_0(\beta, s, G) \quad (11)$$

Using the fact that  $\tan(\frac{\pi}{2} - x) = 1/\tan x$ , following identity for all angles can be established:

$$\tan \beta = \tan \sigma = \frac{1}{\tan \phi_0(\beta, s, G)} \quad (12)$$

or expanding by using (??) and considering only  $\tan \beta$  in the left hand side:

$$\frac{\sin \beta}{\cos \beta} = \frac{2 - G \cos(\beta + s) - G \cos \beta}{G \sin(\beta + s) + G \sin \beta} \quad (13)$$

Let's perform some more simplifications:

$$\begin{aligned} 2 \cos \beta - G \cos(\beta + s) \cos \beta - G \cos \beta \cos \beta &= \\ &= G \sin(\beta + s) \sin \beta + G \sin \beta \sin \beta \\ 2 \cos \beta - G &= G \cos(\beta + s) \cos \beta + G \sin(\beta + s) \sin \beta \\ 2 \cos \beta - G &= G \cos s \end{aligned} \quad (14)$$

Then finally we have synchronous rectification condition:

$$\cos s + 1 = \frac{2}{G} \cos \beta = \frac{2}{G} \cos \sigma \quad (15)$$

It worth noting, that if (15) is satisfied, then the equation for output power  $W$  in model (2) can be simplified even further:

$$W = 4n \frac{\cos s + 1}{\pi^2 Z(\omega)} \sqrt{1 - G \cos(\beta + s)} \quad (16)$$

### 4 Buck mode with $s = 0$

Lets consider first a buck mode with  $s = 0$ , which corresponds to a fully driven converter on primary side and a synchronous rectification on the secondary side. Obviously, buck mode is optimal in terms of  $s \rightarrow \min$ , since 0 is minimal possible value of  $s$ .

From (15) follows that since  $\cos s = 1$ , then

$$\beta = \sigma = \arccos G \quad (17)$$

It immediately follows that in order to have a real solution for  $\beta$ , the voltage ratio should be  $G \leq 1$ , which coincides with the buck mode of converter operation.

To satisfy control goal constraint  $\sigma \geq \sigma_{min}$ , additional consideration should be imposed for voltage ratio  $G$ :

$$\begin{aligned}\sigma &\geq \sigma_{min} \\ \text{acos } G &\geq \sigma_{min} \\ G &\leq \cos(\sigma_{min})\end{aligned}\tag{18}$$

Thus, as long as  $G \leq \cos(\sigma_{min})$ , the buck mode control with  $s = 0$  can satisfy goal constraint  $\sigma \geq \sigma_{min}$ , and voltage ratio  $G = \cos(\sigma_{min})$  is a boundary between buck and boost modes of converter operation.

The output transconductance with feed-forward maps  $\cos \beta = G$  and  $\delta = 0$  can be calculated as after all simplifications using (17) and  $s = 0$ :

$$W = \frac{8n}{\pi^2} \frac{1}{Z(\omega)} \sqrt{1 - G^2}\tag{19}$$

Let's calculate frequency  $\omega$  which is needed to achieve desired output  $W_{ref}$ :

$$\begin{aligned}\frac{8n\sqrt{1 - G^2}}{\pi^2 W_{ref}} &= Z_{ref} \\ Z_{ref} &= \omega L - 1/(\omega C) \\ \omega &= \frac{1}{2LC} \left( \sqrt{C^2 Z_{ref}^2 + 4LC} + C Z_{ref} \right)\end{aligned}\tag{20}$$

## 5 Boost mode with $s > 0$ and buck-boost transition

The boost mode has happened when the buck mode with  $s = 0$  is no longer capable to satisfy the control goal for  $\sigma$ , and as it was established in previous section, for  $G \geq \cos(\sigma_{min})$  a boost mode should be used. In order to satisfy optimality condition  $s \rightarrow \min$ , the  $\sigma$  should be fixed in boost mode, and we have following control problem for angles:

$$\begin{aligned}\delta &= 0 \\ \sigma &= \sigma_{min}\end{aligned}\tag{21}$$

or

$$\sigma = \beta = \sigma_{min}\tag{22}$$

From (15) the shorting time  $s$  is determined by:

$$s = \text{acos}(2 \cos(\sigma_{min})/G - 1)\tag{23}$$

Note for the particular voltage ratio  $G = \cos(\sigma_{min})$ , i.e. exactly at the buck to boost transition border, the  $s = 0$  according to (23), which proofs continuity of  $s(G)$  function. The same is for  $\beta$ , since  $\beta = \text{acos } G$  in buck mode, then at critical voltage ratio  $G = \cos(\sigma_{min})$  we are obtaining  $\beta = \text{acos } \cos(\sigma_{min}) = \sigma_{min}$ , which coincides with continuity of  $\beta(G)$  function.

We can combine  $\beta$  and  $s$  maps for both buck and boost modes by stitching (17), (22) and (23) using minimum and maximum functions (result is pictured in Figure 3):

$$\begin{aligned}\beta &= \text{acos}(\min\{G, G^*\}) \\ s &= \text{acos}\left(\frac{2G^*}{\max\{G, G^*\}} - 1\right)\end{aligned}\tag{24}$$

where

$$G^* = \cos(\sigma_{min})\tag{25}$$

The combined feed-forward control law (both for buck and boost modes) can be formulated as follows:  
For given  $W_{ref}$  and  $G$ , and also pre-calculated buck to boost threshold  $G^* = \cos(\sigma_{min})$ :

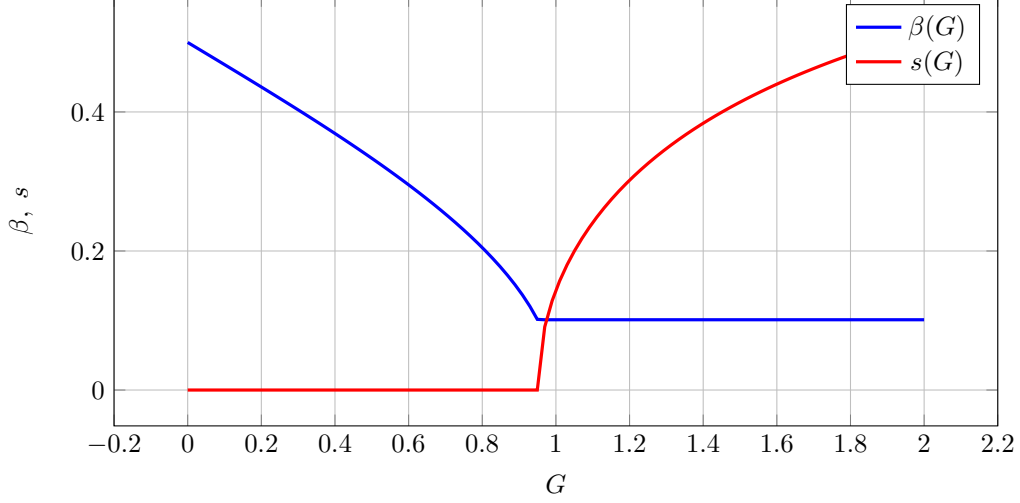


Figure 3: Maps of  $\beta(G)$  and  $s(G)$  for particular  $G^* = 0.95$

1. First calculate the control inputs  $\beta$  and  $s$

$$\begin{aligned}\beta &= \text{acos}(\min\{G, G^*\}) \\ s &= \text{acos}\left(\frac{2G^*}{\max\{G, G^*\}} - 1\right)\end{aligned}\quad (26)$$

2. Then calculate desired tank impedance:

$$Z_{ref} = 4n \frac{\cos s + 1}{\pi^2 W_{ref}} \sqrt{1 - G \cos(\beta + s)} \quad (27)$$

3. The switching frequency will be determined by equation:

$$\omega = \frac{1}{2LC} \left( \sqrt{C^2 Z_{ref}^2 + 4LC} + C Z_{ref} \right) \quad (28)$$

## 6 Low power mode with $\omega = \omega_{max}$

The switching frequency in control (28) is unbounded, i.e. in order to get  $W_{ref} = 0$  frequency should be  $\omega \rightarrow \infty$ . In real systems, the upper frequency is always constrained at  $\omega_{max}$ . Thus if we need output power even lesser than we can get at  $\omega = \omega_{max}$ , impedance can't be further increased and control of output power can be achieved only by commutation parameters  $s$  and  $\beta$  with fixed  $\omega = \omega_{max}$ . This mode we will call a low power mode.

Let's define maximum impedance that we can get:

$$Z_{max} = \omega_{max} L - \frac{1}{\omega_{max} C} \quad (29)$$

The control law for low power can be formulated as follows: for given  $W_{ref}$  find commutation parameters  $\beta, s$  which are satisfying following conditions:

$$\begin{aligned}W_{ref} &= 4n \frac{\cos s + 1}{\pi^2 Z_{max}} \sqrt{1 - G \cos(\beta + s)} \\ \sigma &\geq \sigma_{min} > 0\end{aligned}\quad (30)$$

Let's consider an idea to limit output power by additional increase of  $s$ , which is equivalent to dimming the output down to zero power at  $s = \pi$  when secondary side is completely shorted. Just to mention that an

another possibility for output power regulation at constant frequency is to shift the secondary side respect to primary side by introducing  $\delta > 0$ .

As stated by equation (15), for any arbitrary  $s$  in synchronous rectification:

$$\cos \beta = \frac{G}{2}(\cos s + 1) \quad (31)$$

By using equation (15) and denoting  $x = \cos s$  the equation (30) can be simplified down to:

$$W_{ref} = 2\sqrt{2}n \frac{x+1}{\pi^2 Z_{max}} \sqrt{G\sqrt{(1-x^2)(4-G^2(x+1)^2)} - G^2x(x+1) + 2} \quad (32)$$

which is algebraic respect to  $x$ .

To characterize dependency of  $W$  from  $s$  with fixed frequency, lets try to calculate (32) for different values of  $G$ . Let's denote  $s_0$  and  $\beta_0$  as commutation parameters obtained by (26) without any additional secondary side shorting for low power. Likewise, let's denote  $W_0$  the output power obtained for fixed maximal frequency  $\omega_{max}$ , but without any additional secondary side shorting for low power.

$$W_0 = 4n \frac{\cos s_0 + 1}{\pi^2 Z_{max}} \sqrt{1 - G \cos(\beta_0 + s_0)} \quad (33)$$

The output power variation for different values of  $G$  is demonstrated in Figure 4 as ratio of  $W/W_0$ . As one can see from the picture, the zero power operation  $W = 0$  is achieved for  $s = \pi$  (fully shorted secondary side) regardless of  $G$ . But an interesting feature of the system is that  $W = W_0$  can be seen for the values  $s > 0$  even in buck mode. That means that the characteristic  $W(s)$  is non-monotonic, and a discontinuous control will be applied for  $s$  when transitioning from regular operation (with  $W_0$  output power) to a low power operation with  $W < W_0$ . This feature will be addressed separately later.

The final algorithm for feed-forward map calculations in low power mode is formulated as follows:

*If calculated switching frequency in control (28) greater than  $\omega_{max}$  to obtain a desired  $W_{ref}$ , then*

*1. Numerically solve following equation for  $x$ :*

$$2\sqrt{2}n \frac{x+1}{\pi^2 Z_{max}} \sqrt{G\sqrt{(1-x^2)(4-G^2(x+1)^2)} - G^2x(x+1) + 2} = W_{ref} \quad (34)$$

*The solution can be obtained using bisection (dichotomy) method by ranging  $x \in [-1, \cos s_0]$ .*

*2. Calculate switching parameters as follows:*

$$\begin{aligned} s &= \arccos x \\ \beta &= \arccos \left( G \cdot \frac{x+1}{2} \right) \end{aligned} \quad (35)$$

## 7 Feed-forward control simulations

The series of simulations were carried out in order to proof the concept of feed-forward inversion algorithms for plant (2). The Simulink simulation model demonstrated in Figure 5 uses FHA model of form (2) with coefficients (??) and (4), which is implemented in *MATLAB Function [tank steady-state]* block. The feed-forward calculations (26) and (28) for buck and boost modes, along with low-power mode (34) are implemented in *MATLAB Function [feed-forward map]* block.

The tank parameters are:  $L = 125 \text{ uH}$  and  $C = 45 \text{ nF}$ , turn ratio  $n = 20$  and maximum frequency  $f_{max} = 300 \text{ kHz}$ .

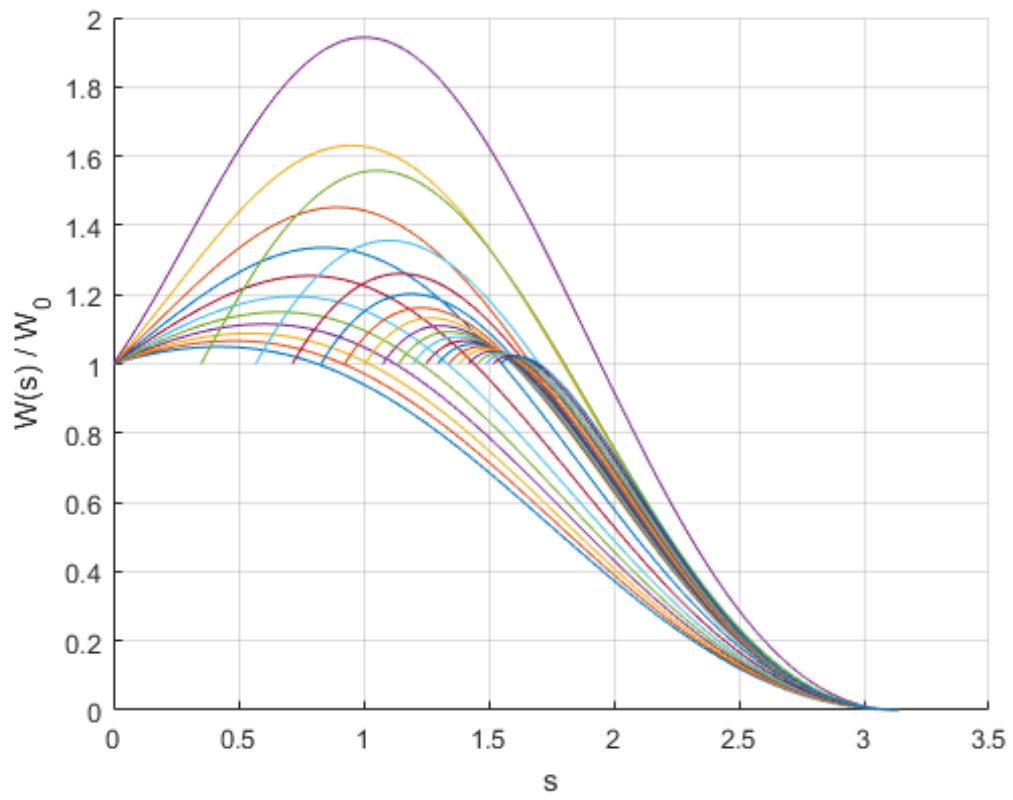


Figure 4: Output power variation with  $s$  ranging from  $s_0$  to  $\pi$  for  $0.4 \geq G \geq 1.8$

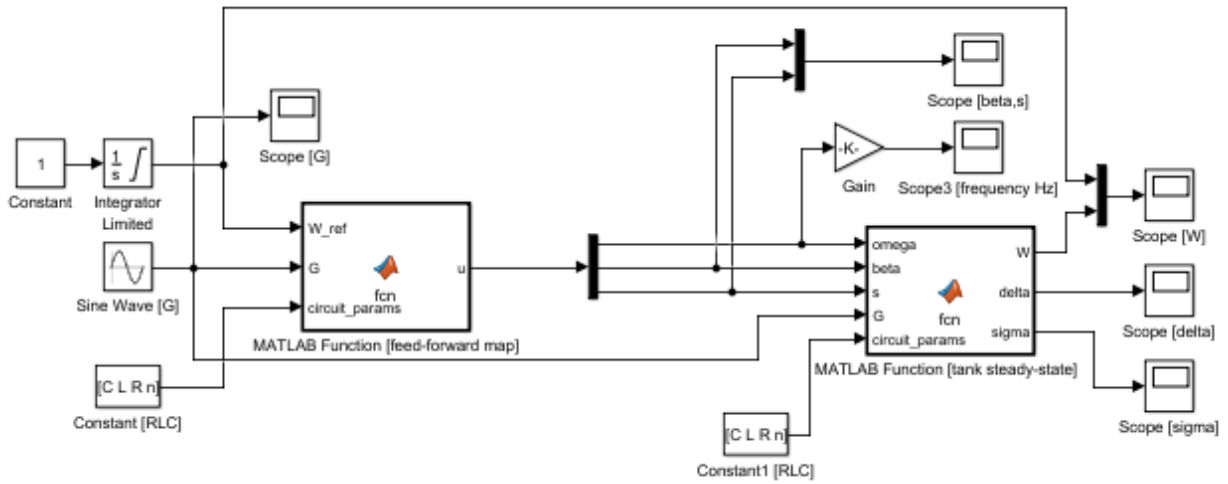


Figure 5: Simulink model for testing feed-forward control only

To test both buck and boost mode, the voltage ration  $G$  varied in boundaries between  $G \in [0.25, 1.75]$  as pictured in Figure (6).

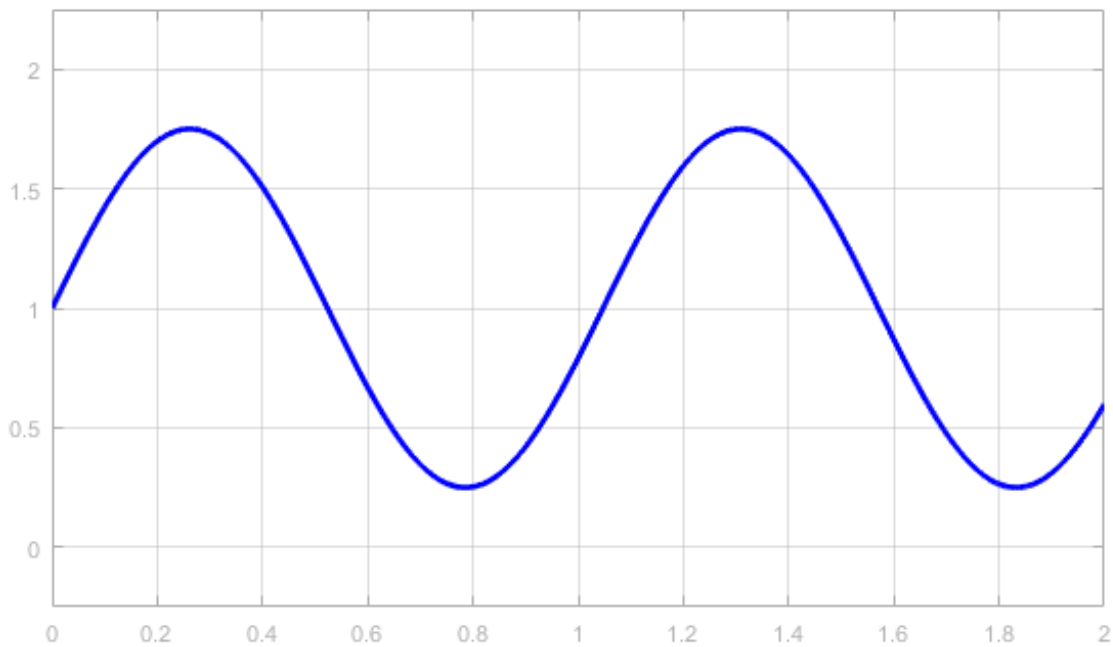


Figure 6: Variation of voltage ratio  $G$  during simulation

The result of the simulation (Figure 7) demonstrates an exact reference following by output  $W$ .

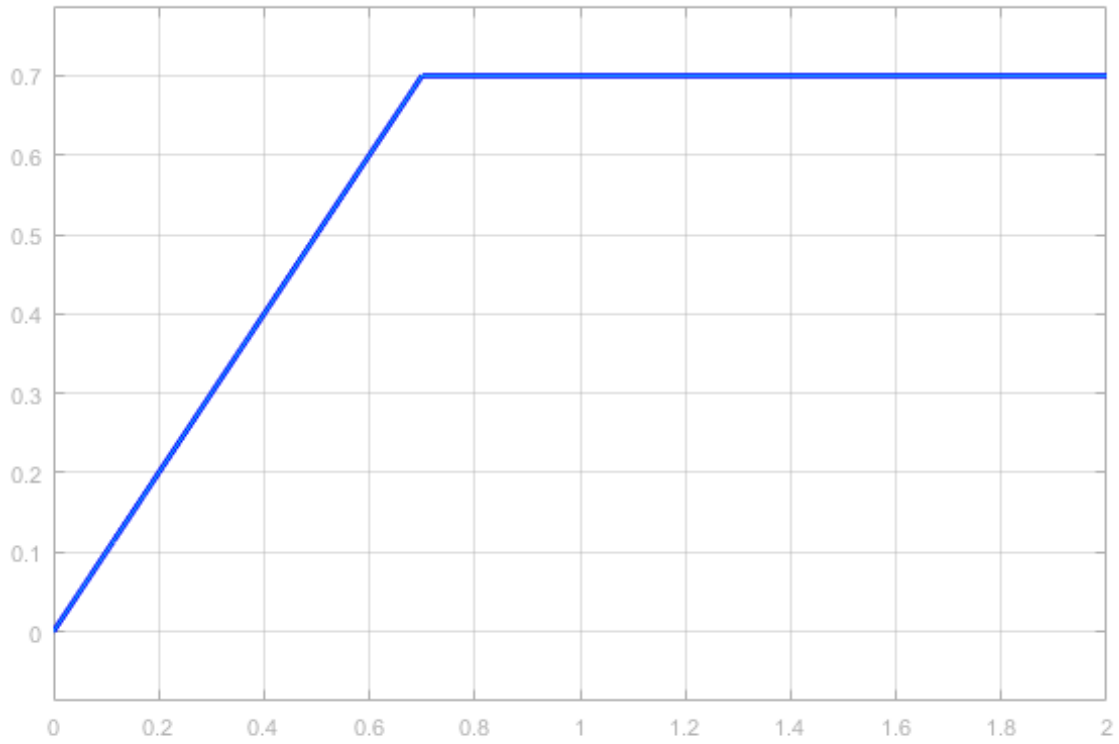


Figure 7: Reference and plant output  $W$

The dynamics of plant inputs obtained by control algorithms are demonstrated in Figures 8 and 9.

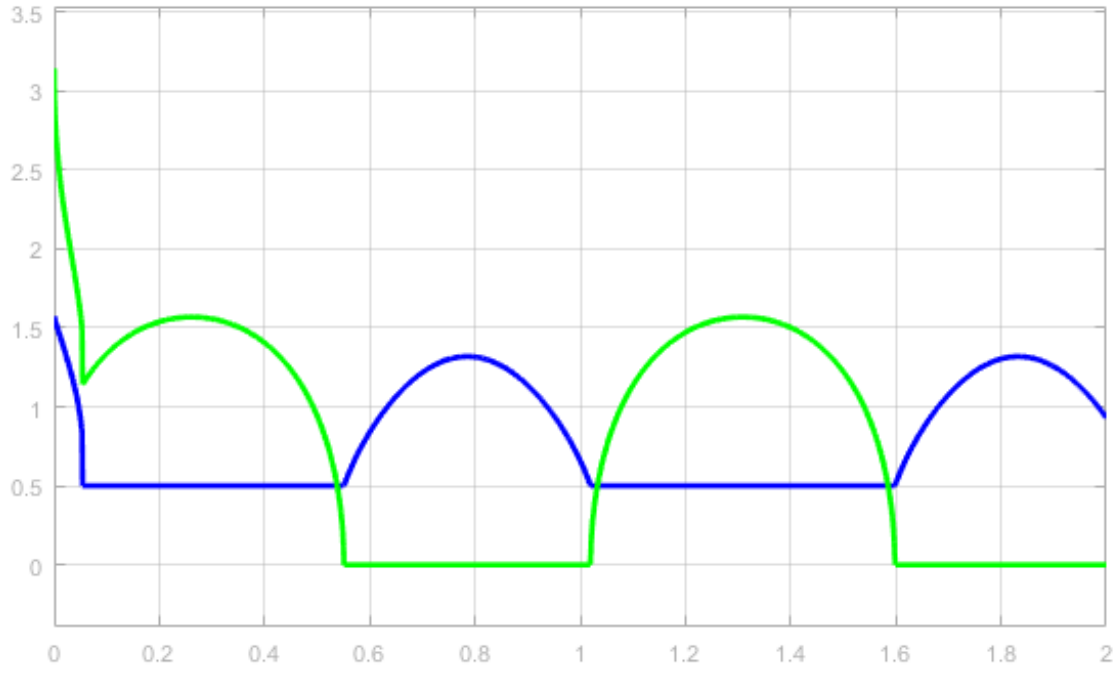


Figure 8: Commutation parameters  $\beta$  and  $s$

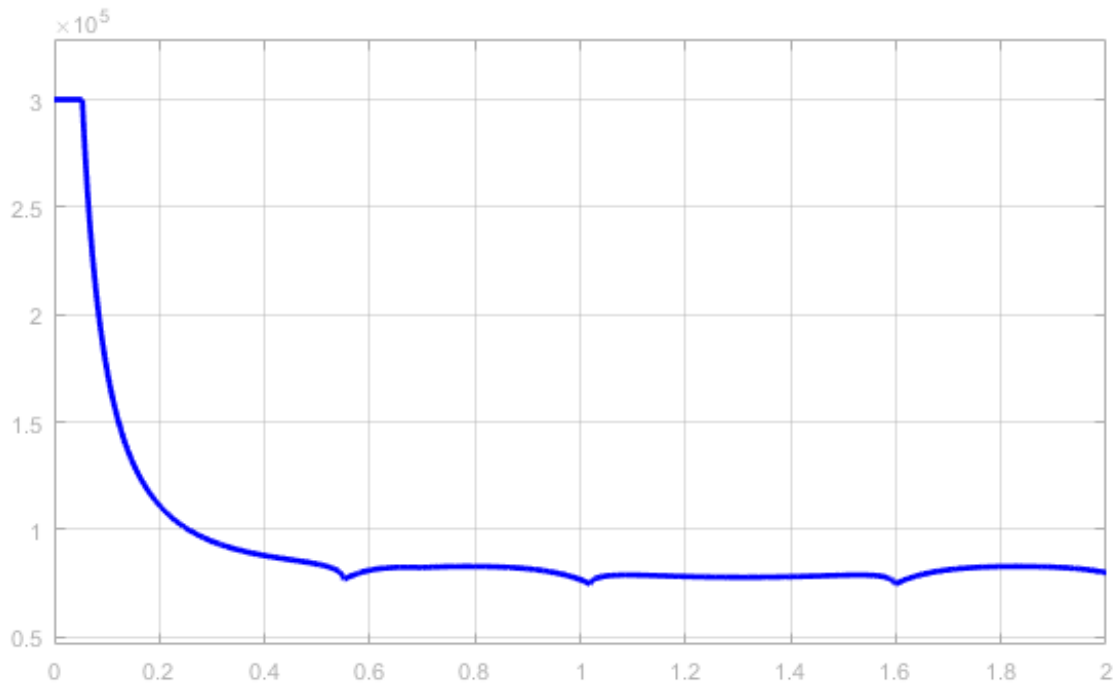


Figure 9: Frequency  $2\pi\omega$

## 8 Closed-loop control simulations

Obviously, the feed-forward control algorithm is not directly applicable to the real systems because of model uncertainties. The feedback loops should be added to the control scheme.

First, the power regulator will be in form:

$$W_{desired} = PI[W_{ref} - W_{out}] + W_{ref} \quad (36)$$

where  $W_{desired}$  is an input to the feed-forward control algorithm,  $W_{ref}$  is the reference setpoint signal (like a ramp with saturation in this particular simulation), and  $W_{out}$  is real output of the plant,  $PI[e]$  is PI-regulator with error input  $e$ . Worth noting that in a real system this control loop would regulate current  $I_{out}$  and transition to the transconductance  $W$  will be based on measured input voltage  $V_{in}$  as  $W = I_{out}/V_{in}$ .

An additional regulator would be for driving  $\delta$  to 0. From model equation (2) for  $\delta$ , it is obvious that  $\beta$  is influencing almost linear to the  $\delta$  if we are neglecting variation of  $\phi_0$  (which should be made with some caution).

$$\beta = PI[\delta_{ref} - \delta_{out}] + \beta_{ff} \quad (37)$$

where  $\beta$  is input to the plant (commanded phase shift),  $\delta_{ref} = 0$  is a reference setpoint for the actual secondary side alignment,  $\delta_{out}$  is measured misalignment between secondary side and switching and tank current sign,  $\beta_{ff}$  is value of  $\beta$  determined by feed-forward control (26), (28) and (34).

The Simulink simulation model demonstrated in Figure 10.

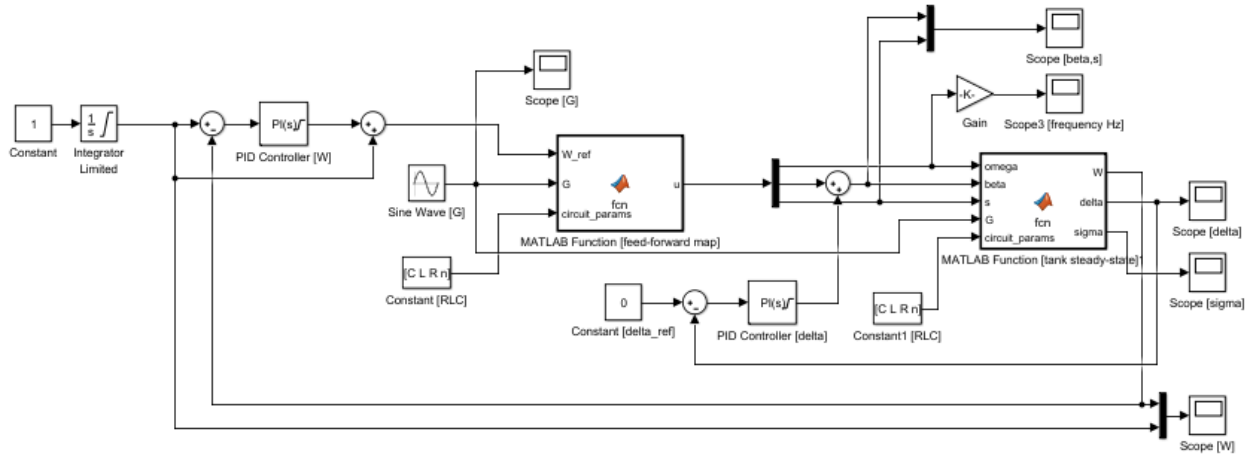


Figure 10: Simulink model for testing closed loop control respect to  $W$  and  $\delta$

This time we will also change the tank parameters by introducing in it a series resistance  $R = 670$  mOhm, and decreasing inductance by 10%:  $L = 112.5$  uH.

The variation of the  $G$  will be the same for purely feed-forward control test between  $G \in [0.25, 1.75]$  as it pictured in Figure (6)

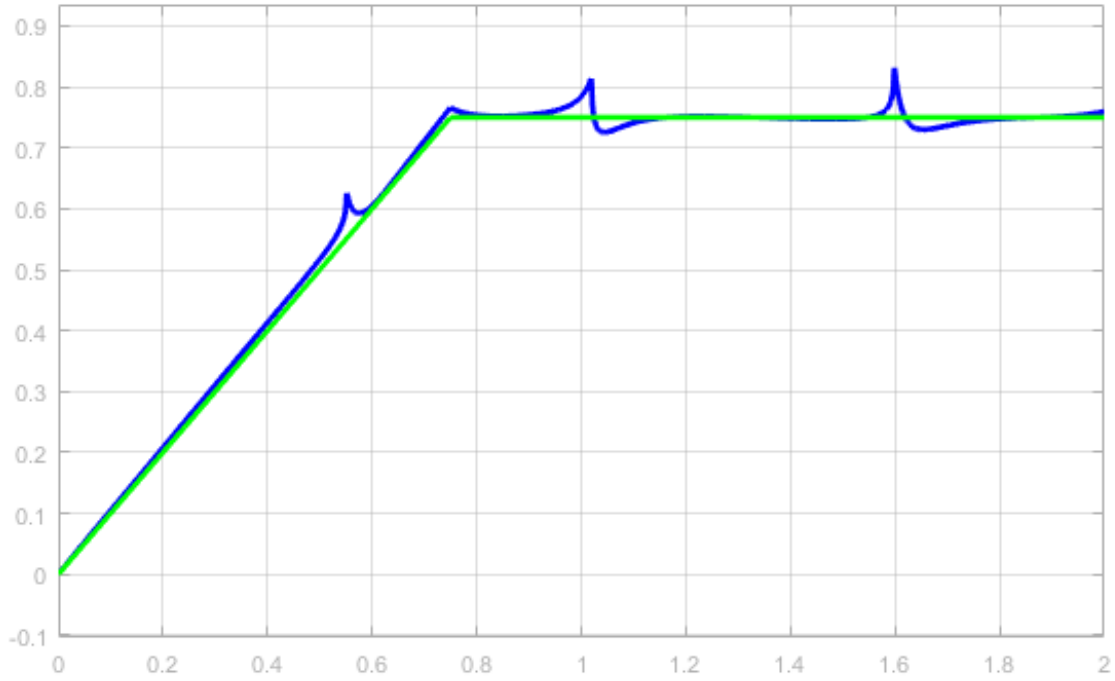


Figure 11: Reference and plant output  $W$

As it seen from response  $W$  (Figure 11), the plant output is not following reference signal exactly, but stays within a boundary around it.

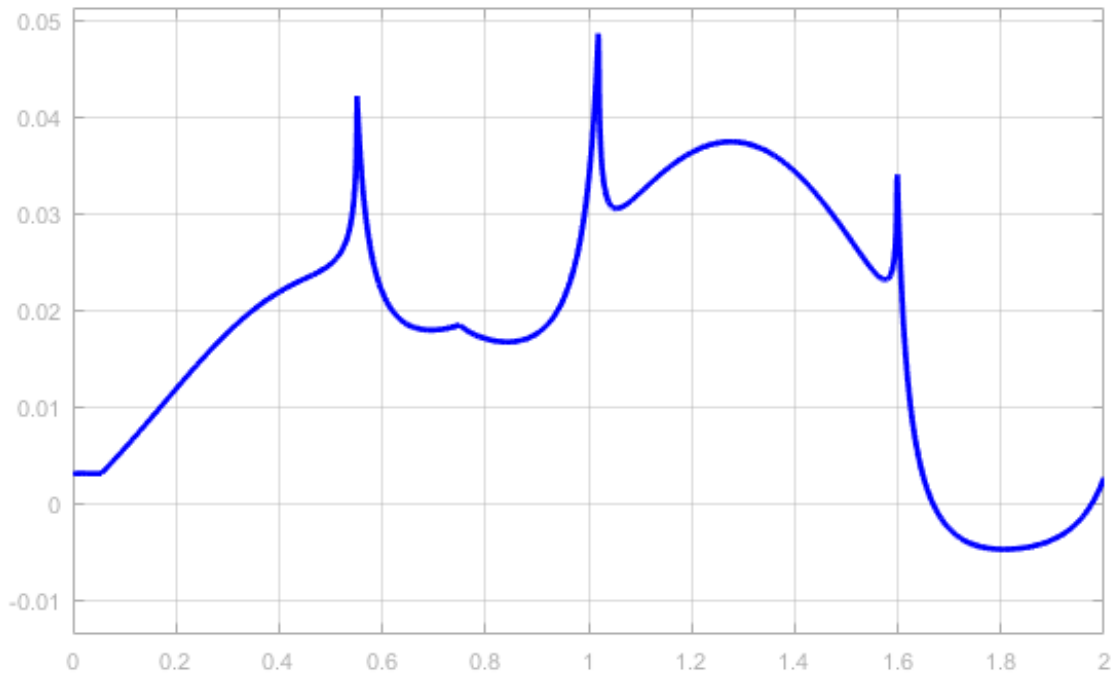


Figure 12: Output  $\delta$ , the reference value is  $\delta^* = 0$

The same thing is for  $\delta$  which is not 0 all the time because of feed-forward controller and plant discrepancy. But controller tries to compensate it with an action for  $\beta$ .

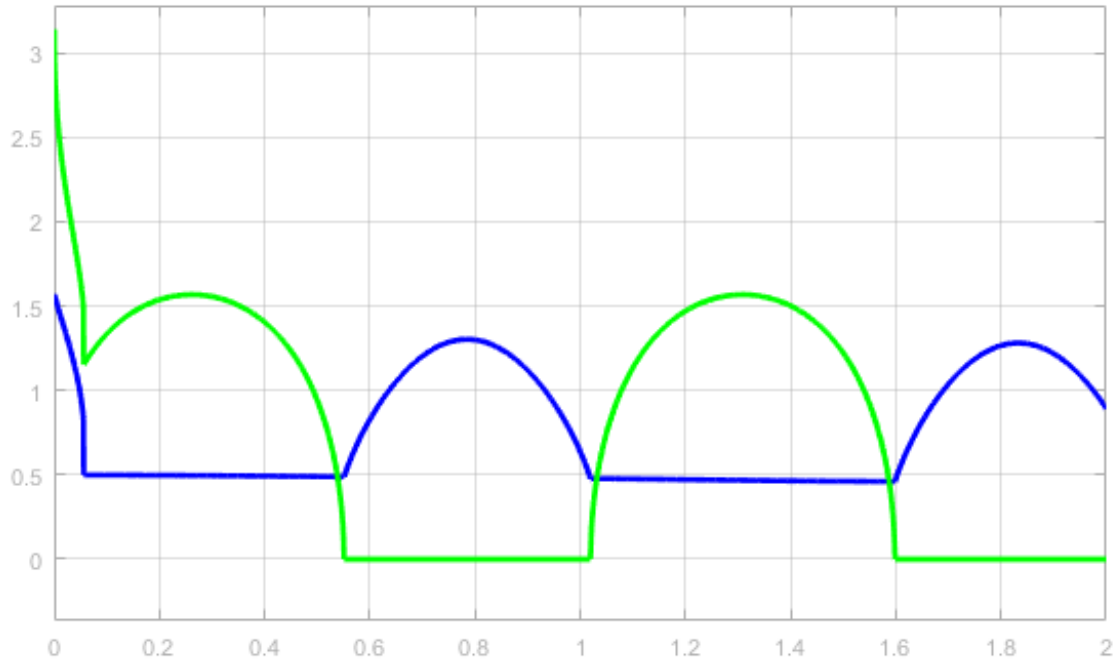


Figure 13: Commutation parameters  $\beta$  and  $s$

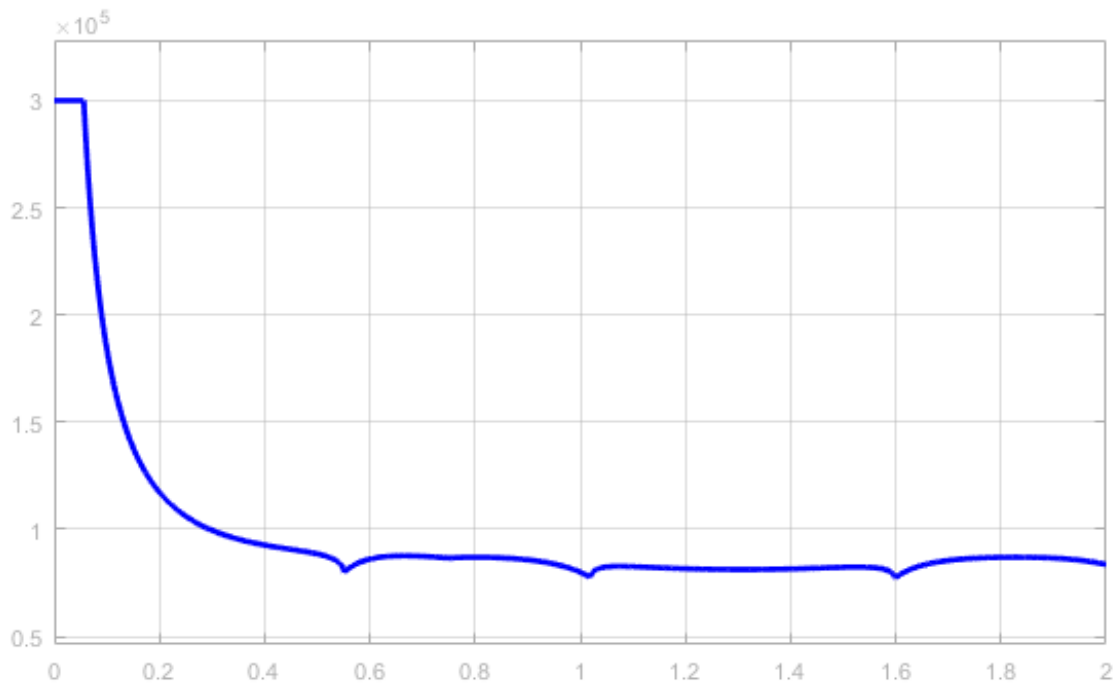


Figure 14: Frequency  $2\pi\omega$

## References

- [1] Li, X. and Bhat, A.K., 2010. Analysis and design of high-frequency isolated dual-bridge series resonant DC/DC converter. *IEEE Transactions on Power Electronics*, 25(4), pp.850-862.
- [2] Krismer, F., Biela, J. and Kolar, J.W., 2005, October. A comparative evaluation of isolated bi-directional DC/DC converters with wide input and output voltage range. In *Industry Applications Conference, 2005. Fourtieth IAS Annual Meeting. Conference Record of the 2005 (Vol. 1, pp. 599-606)*. IEEE.
- [3] Wang, C.S., Li, W., Wang, Y.F., Han, F.Q., Meng, Z. and Li, G.D., 2017. An Isolated Three-Port Bidirectional DC-DC Converter with Enlarged ZVS Region for HESS Applications in DC Microgrids. *Energies*, 10(4), p.446.
- [4] Zhao, B., Song, Q., Liu, W. and Sun, Y., 2014. Overview of dual-active-bridge isolated bidirectional DCDC converter for high-frequency-link power-conversion system. *IEEE Transactions on Power Electronics*, 29(8), pp.4091-4106.
- [5] <https://www.fairchildsemi.com/application-notes/AN/AN-4151.pdf>
- [6] Hu, S., Li, X., Lu, M. and Luan, B.Y., 2015. Operation Modes of a Secondary-Side Phase-Shifted Resonant Converter. *Energies*, 8(11), pp.12314-12330.
- [7] Jiang, M. and Li, W., 2014. A Soft-Switching Control Method of Isolated LC Series Resonant Transformer Full Bridge DCDC Converter. In *Proceedings of the 2013 International Conference on Electrical and Information Technologies for Rail Transportation (EITRT2013)-Volume II (pp. 11-20)*. Springer, Berlin, Heidelberg.
- [8] Wu, H., Wang, P. and Li, Y., 2014, August. A control method for series resonant dual active bridge DC/DC converter. In *Transportation Electrification Asia-Pacific (ITEC Asia-Pacific), 2014 IEEE Conference and Expo (pp. 1-5)*. IEEE.
- [9] Hu, G.-Y.; Li, X.; Luan, B.-Y., 2014. A Generalized Approach for the Steady-State Analysis of Dual-Bridge Resonant Converters. *Energies* 2014, 7, 7915-7935.
- [10] Chen, H. and Bhat, A.K., 2016, May. A bidirectional dual-bridge LCL-type series resonant converter controlled with modified gating scheme. In *Power Electronics and Motion Control Conference (IPEM-ECCE Asia), 2016 IEEE 8th International (pp. 3036-3042)*. IEEE.
- [11] Aboushady, A.A., Ahmed, K., Finney, S.J. and Williams, B.W., 2010. Steady-state analysis of full-bridge series resonant converter with phase-shift and frequency control. In *Power Electronics, Machines and Drives (PEMD 2010), 5th IET International Conference on, 2010, pp 1-6*.
- [12] Oruganti, R., 1987. State-plane analysis of resonant converters (Doctoral dissertation, Virginia Polytechnic Institute and State University).
- [13] Rossetto, L., 1996. A simple control technique for series resonant converters. *IEEE Transactions on Power Electronics*, 11(4), pp.554-560.
- [14] Chen, H., Sng, E.K.K. and Tseng, K.J., 2006. Generalized optimal trajectory control for closed loop control of series-parallel resonant converter. *IEEE transactions on power electronics*, 21(5), pp.1347-1355.
- [15] Feng, W., Lee, F.C. and Mattavelli, P., 2013. Simplified optimal trajectory control (SOTC) for LLC resonant converters. *IEEE Transactions on Power Electronics*, 28(5), pp.2415-2426.
- [16] Sarnago, H., Lucia, O., Mediano, A. and Burdio, J.M., 2015. Analytical model of the half-bridge series resonant inverter for improved power conversion efficiency and performance. *IEEE Transactions on Power Electronics*, 30(8), pp.4128-4143.
- [17] Jiang, J., Bao, Y. and Wang, L.Y., 2014. Topology of a bidirectional converter for energy interaction between electric vehicles and the grid. *Energies*, 7(8), pp.4858-4894.

- [18] Zhao, X., Zhang, L., Born, R. and Lai, J.S., 2017. A high-efficiency hybrid resonant converter with wide-input regulation for photovoltaic applications. *IEEE Transactions on Industrial Electronics*, 64(5), pp.3684-3695.
- [19] Riedel, J. 2017. On frequency domain analysis of dual active bridge dc-dc converters. Ph.D. thesis, RMIT Melbourne,. Dissertation, March 2017.
- [20] Xiao, Y., Zhang, Z., Mao, X., Manez, K.T. and Andersen, M.A., 2018, March. Power plateau and anti-power phenomenon of dual active bridge converter with phase-shift modulation. In *Applied Power Electronics Conference and Exposition (APEC), 2018 IEEE* (pp. 1871-1875). IEEE.
- [21] Shen, Y., Wang, H., Al-Durra, A., Qin, Z. and Blaabjerg, F., 2018. A Bidirectional Resonant DCDC Converter Suitable for Wide Voltage Gain Range. *IEEE Transactions on Power Electronics*, 33(4), pp.2957-2975.
- [22] Borisevich, A., and Gleyzer, F., 2019. Model of DC/DC Dual-Bridge Series Resonant Converter in Buck and Boost Modes for Output Current and Commutation Timing Control. *Journal of Engineering Science and Technology Review* 12.2 (2019): 152-160.